Communications on Applied Mathematics and Computation
https://doi.org/10.1007/s42967-019-0002-2

ORIGINAL PAPER

Solving Interface Problems of the Helmholtz Equation by Immersed Finite Element Methods

Tao Lin[1] · Yanping Lin[2] · Qiao Zhuang[1]

Received: 18 May 2018 / Revised: 19 November 2018 / Accepted: 23 November 2018

Abstract
This article reports our explorations for solving interface problems of the Helmholtz equation by immersed finite elements (IFE) on interface independent meshes. Two IFE methods are investigated: the partially penalized IFE (PPIFE) and discontinuous Galerkin IFE (DGIFE) methods. Optimal convergence rates are observed for these IFE methods once the mesh size is smaller than the optimal mesh size which is mainly dictated by the wave number. Numerical experiments also suggest that higher degree IFE methods are advantageous because of their larger optimal mesh size and higher convergence rates.

Keywords Helmholtz interface problems · Immersed finite element (IFE) methods · Higher degree finite element methods

Mathematics Subject Classification 65N30 · 65N50 · 35R05

1 Introduction

Wave propagation in composite media formed with different materials appears in many areas of science and engineering, for example, the study of the wave diffraction [10, 50], wave scattering [16, 55], and wave reflection/transmission [18, 36], to name just a few. In a suitable physical configuration, the amplitude of the wave can be described by the Helmholtz equation. In addition, across the interface between two different materials, the amplitude is required to satisfy the jump conditions [35, 57] imposed according to pertinent physics, such as the continuity of pressure, the normal velocity or volume flow [18, 35, 36, 54]. These considerations lead to the following *interface problem* for the Helmholtz

✉ Yanping Lin
yanping.lin@polyu.edu.hk

Tao Lin
tlin@vt.edu

Qiao Zhuang
qzhuang@vt.edu

[1] Department of Mathematics, Virginia Tech, Blacksburg, VA 24061, USA

[2] Department of Applied Mathematics, Hong Kong Polytechnic University, Kowloon, Hong Kong, China

Published online: 09 May 2019

equation [13, 37] posed in a domain $\Omega \subseteq \mathbb{R}^2$ divided by an interface curve Γ into two subdomains Ω^1 and Ω^2 each occupied a different material: find $u(X)$ such that

$$-\nabla \cdot (\beta \nabla u) - w^2 u = f \quad \text{in } \Omega = \Omega^1 \cup \Omega^2, \tag{1a}$$

$$\beta \frac{\partial u}{\partial \boldsymbol{n}_\Omega} + \mathrm{i} w u = g \quad \text{on } \partial\Omega, \tag{1b}$$

together with the jump conditions across the interface [13, 18, 35–37]:

$$[u]_\Gamma := u^1|_\Gamma - u^2|_\Gamma = 0, \tag{1c}$$

$$\left[\beta \nabla u \cdot \mathbf{n}\right]_\Gamma := \beta_1 \nabla u^1 \cdot \mathbf{n}|_\Gamma - \beta_2 \nabla u^2 \cdot \mathbf{n}|_\Gamma = 0, \tag{1d}$$

where $u^s = u|_{\Omega^s}, s = 1, 2$ and $\mathbf{n}$ is the unit normal vector to the interface Γ. In this interface problem, (1b) specifies the first order absorb boundary condition with $\mathrm{i} = \sqrt{-1}$, w is the wave number, $\mathbf{n}_\Omega$ is the unit outward normal vector to $\partial\Omega$, and the coefficient β is a piecewise positive constant function such that

$$\beta(X) = \begin{cases} \beta_1 & \text{for } X \in \Omega^1, \\ \beta_2 & \text{for } X \in \Omega^2. \end{cases}$$

The Helmholtz boundary value problems (BVPs) without interface have been widely studied using numerical methods, among which, are the classic finite element methods [6, 8, 21, 33]. More sophisticated finite element methods such as the interior penalty Galerkin (IPG) method [14, 22] and discontinuous Galerkin (DG) method (including interior penalty DG, IPDG for abbreviation) [23–25, 38, 46, 47] have been developed for solving Helmholtz boundary value problems.

Finite element methods such as those mentioned above can be applied to solve interface problems provided that they use a body-fitting mesh [7, 12, 17, 53] in which each element is essentially on one side of the interface or each element is occupied by one of the materials. However, this body-fitting requirement can hinder a finite element method in some applications such as a simulation in which an interface problem has to be solved repeatedly for different geometries and locations of the interface which demand the mesh to be regenerated again and again to accommodate the change of the material interface. For such simulations, numerical methods based an interface-independent mesh are often preferred. For example, extended finite element methods (X-FEM), immersed interface methods (IIM), and multi-scale methods have been developed to solve interface problems of elliptic partial differential equations with an interface-independent mesh, and readers are referred to [5, 9, 19, 32, 39, 40] for more details about these methods. In particular, some of these methods have been applied to Helmholtz interface problems, see [55] for IIM and [57] for X-FEM.

The immersed finite element (IFE) methods are another class of finite element methods developed to solve interface problems with interface-independent meshes. With Hesie-Clough–Tocher type [11, 20] macro polynomials constructed according to the interface jump conditions as the local shape functions, IFE methods allow the interface to split the interior of the elements in a mesh; therefore, IFE methods are interface-independent methods that can use highly structured Cartesian meshes for problems with non-trivial interfaces, see [41, 42, 51] for some IFE spaces based on triangular Cartesian meshes and [26, 29, 31, 43] for some IFE spaces based rectangular Catesian meshes. Partially penalized IFE (PPIFE) and DGIFE methods [27, 30, 31, 44, 45, 56] have been developed for elliptic interface problems, and the related extensions to higher degree IFE methods are presented in [1–3, 48].

The purpose of this article is to report our exploration for applying IFE methods to the Helmholtz interface problem described by (1a)–(1d). Since the Helmholtz equation contains the elliptic operator and the interface jump conditions specified in (1c) and (1d) are the same as those for the elliptic interface problems, it is natural for us to consider IFE methods for the Helmholtz interface problem by using the IFE spaces constructed for the elliptic interface problems. Both the partially penalized Galerkin formulation and the discontinuous Galerkin formulation will be considered. We will also explore higher degree IFE methods because it is well known that higher degree finite element methods have desirable features for wave propagation problems [4, 15, 49], such as reducing the numerical dispersion and errors in solution due to the pollution effect caused by a large wave number [34, 52]. Additionally, it was found out that employing higher degree finite elements requires less degrees of freedom for numerical solutions to attain a specific accuracy [34]. Specifically, the layout of this article is as follows: in Sect. 2, we introduce the notation and assumptions to be used in this article, and we recall the IFE spaces in the literature. In Sect. 3, PPIFE and DGIFE schemes are derived for the Helmholtz interface problem (1). In Sect. 4, we present numerical examples to show the features of the proposed IFE methods. Some concise conclusions and remarks are given in Sect. 5.

2 IFE Spaces

Given a polygonal domain $\Omega \subset \mathbb{R}^2$, we let $\mathcal{T}_h$ be a triangular or a rectangular mesh of Ω, and we use $\mathcal{E}_h$ to denote the set of edges in $\mathcal{T}_h$. Without loss of generality, we assume that the interface Γ does not intersect with $\partial\Omega$. Since the mesh $\mathcal{T}_h$ is assumed to be independent of the interface Γ, some elements in the mesh $\mathcal{T}_h$ will be inevitably cut by Γ. Depending on whether an element intersects with the material interface Γ or not, elements in the mesh $\mathcal{T}_h$ are categorized as interface elements and non-interface elements, and we use $\mathcal{T}_h^{\mathrm{i}}$ to denote the set of interface elements and use $\mathcal{T}_h^{\mathrm{n}}$ for the set of non-interface elements. Similarly, edges in the mesh $\mathcal{T}_h$ are also classified as interface edges and non-interface edges, and we will use $\mathcal{E}_h^{\mathrm{i}}$ and $\mathcal{E}_h^{\mathrm{n}}$ for the set of interface edges and the set of non-interface edges, respectively. In addition, we will use $\mathcal{E}_h^{\mathrm{b}}$ for the set of boundary edges, and use $\mathring{\mathcal{E}}_h$, $\mathring{\mathcal{E}}_h^{\mathrm{i}}$ and $\mathring{\mathcal{E}}_h^{\mathrm{n}}$ for the set of interior edges, the set of interior interface edges, and the set of interior non-interface edges, respectively. As usual, [26, 28, 31], we adopt the following assumptions about the mesh $\mathcal{T}_h$:

(H1) The interface Γ cannot intersect an edge of any element at more than two points unless the edge is part of Γ.
(H2) If Γ intersects the boundary of an element at two points, these intersection points must be on different edges of this element.
(H3) The interface Γ is a piecewise C^2 function, and for every interface element $T \in \mathcal{T}_h^{\mathrm{i}}$, $\Gamma \cap T$ is C^2.

In the discussion from now on, we will use the following function spaces. For an open set $\tilde{\Omega} \subseteq \Omega$, we let $H^p(\tilde{\Omega}), p \geq 0$ be the standard Sobolev space. Furthermore, if $\tilde{\Omega}^s = \tilde{\Omega} \cap \Omega^s \neq \emptyset$, $s = 1, 2$, we let

$$PH^p(\tilde{\Omega}) = \left\{ u : u|_{\tilde{\Omega}^s} \in H^p(\tilde{\Omega}^s),\ s = 1, 2;\ [u] = 0,\ [\beta \nabla u \cdot \mathbf{n}_\Gamma] = 0 \text{ on } \Gamma \cap \tilde{\Omega} \right\},\ p \geq 2.$$

We will also use $\mathbb{P}^k$ to denote the space of polynomials with degree not more than an integer $k \geq 0$, and let $\mathbb{Q}^1$ be the space of bilinear polynomials.

2.1 Local Linear and Bilinear IFE Spaces

We now recall the lower degree local IFE spaces, i.e., the local IFE spaces constructed with linear or bilinear polynomials. We start from the linear case. For each element $T = \Delta A_1A_2A_3$ in a triangular mesh $\mathcal{T}_h$, we let $\psi_{j,T}, j = 1, 2, 3$ be the standard linear finite element shape functions associated with the vertices $A_j, j = 1, 2, 3$. When $T = \Delta A_1A_2A_3 \in \mathcal{T}_h^{\mathrm{i}}$, we denote the intersection points of the interface Γ and ∂T by D and E, see the left illustration in Fig. 1. The line $l = \overline{DE}$ partitions T into two sub-elements: T_l^1 and T_l^2. We let

$$\mathcal{P}^1(T) = \{q \ : \ q|_{T_l^s} \in \mathbb{P}^1, s = 1, 2\}.$$

Then, the linear IFE shape functions on $T = \Delta A_1A_2A_3$ are defined as piecewise linear functions in $\mathcal{P}^1(T)$ [41, 42] such that

$$\phi_{i,T}(x,y) = \begin{cases} \phi_{i,T}^-(x,y) = a^-x + b^-y + c^-, & \text{if } (x,y) \in T_l^1, \\ \phi_{i,T}^+(x,y) = a^+x + b^+y + c^+, & \text{if } (x,y) \in T_l^2, \\ \phi^-(D) = \phi^+(D), \phi^-(E) = \phi^+(E), \\ \beta^+ \frac{\partial \phi^+}{\partial \boldsymbol{n}_{\overline{DE}}} - \beta^- \frac{\partial \phi^-}{\partial \boldsymbol{n}_{\overline{DE}}} = 0, \end{cases} \tag{2}$$

$$\phi_{i,T}(A_j) = \delta_{ij}, \quad \forall i, j \in \{1, 2, 3\}. \tag{3}$$

We note that the third and the fourth equations in (2) follow from the interface jump conditions (1c) and (1d) for the Helmholtz interface problems which happen to be the same as those for the elliptic interface problems discussed in [41, 42] where existence and uniqueness of linear IFE shape functions on a triangular interface element have been proved. Thus, the local linear IFE space on each element T in a triangular mesh $\mathcal{T}_h$ is defined as

$$S_h^1(T) = \begin{cases} \text{Span}\{\psi_{i,T}, i = 1, 2, 3\} = \mathbb{P}^1, & T \in \mathcal{T}_h^{\mathrm{n}}, \\ \text{Span}\{\phi_{i,T}, i = 1, 2, 3\}, & T \in \mathcal{T}_h^{\mathrm{i}}. \end{cases} \tag{4}$$

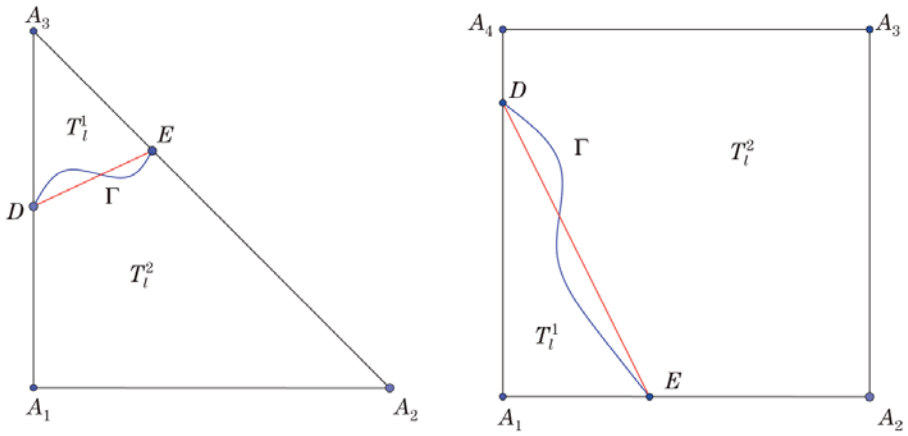

Fig. 1 Left: triangular interface element; right: rectangular interface element

Similarly, for a typical rectangular element $T = \square A_1A_2A_3A_4$, we let $\psi_{j,T}, j = 1, 2, 3, 4$ be the standard bilinear finite element shape functions associated with the vertices $A_j, j = 1, 2, 3, 4$. When $T = \square A_1A_2A_3A_4 \in \mathcal{T}_h^{\mathrm{i}}$, we denote the intersection points of the interface Γ and ∂T by D and E, see the right illustration in Fig. 1. The line $l = \overline{DE}$ partitions T into two sub-elements: T_l^1 and T_l^2, and we can use them to define the following space of piecewise bilinear polynomials:

$$\mathcal{Q}^1(T) = \{q \ : \ q|_{T_l^s} \in \mathbb{Q}^1, s = 1, 2\}.$$

Then, the local bilinear IFE shape functions are defined as the piecewise bilinear functions in $\mathcal{Q}^1(T)$ [26, 31, 43] such that

$$\phi_{i,T}(x,y) = \begin{cases} \phi_{i,T}^-(x,y) = a^-x + b^-y + c^- + d^-xy, & \text{if } (x,y) \in T_l{}^1, \\ \phi_{i,T}^+(x,y) = a^+x + b^+y + c^+ + d^+xy, & \text{if } (x,y) \in T_l{}^2, \\ \phi^-(D) = \phi^+(D), \phi^-(E) = \phi^+(E), d^- = d^+, \\ \int_{\overline{DE}} \left(\beta^+ \frac{\partial \phi^+}{\partial \boldsymbol{n}_{\overline{DE}}} - \beta^- \frac{\partial \phi^-}{\partial \boldsymbol{n}_{\overline{DE}}} \right) \mathrm{d}s = 0, \end{cases} \tag{5}$$

$$\phi_{i,T}(A_j) = \delta_{ij}, \quad \forall i, j \in \{1, 2, 3, 4\}. \tag{6}$$

The existence and uniqueness of bilinear IFE shape functions on a rectangular interface element have been proved in [26, 31]. Thus, the local bilinear IFE space on each element T in a rectangular mesh $\mathcal{T}_h$ is defined as

$$S_h^1(T) = \begin{cases} \mathrm{Span}\{\psi_{i,T}, i = 1, 2, 3, 4\} = \mathbb{Q}^1(T), & T \in \mathcal{T}_h^{\mathrm{n}}, \\ \mathrm{Span}\{\phi_{i,T}, i = 1, 2, 3, 4\}, & T \in \mathcal{T}_h^{\mathrm{i}}. \end{cases} \tag{7}$$

2.2 Higher Degree IFE Spaces

We now recall higher degree IFE functions based on a triangular mesh $\mathcal{T}_h$. For each interface element $T \in \mathcal{T}_h^{\mathrm{i}}$, we use the interface curve Γ to partition it into two sub-elements T^1 and T^2, then, we use these two sub-elements to define the following space of k-th degree piecewise polynomials:

$$\mathcal{P}^k(T) = \{q \ : \ q|_{T^s} \in \mathbb{P}^k, s = 1, 2\}, \quad k \geq 2.$$

Higher degree IFE functions are constructed by functions in $\mathcal{P}^k(T), k \geq 2$, but the construction procedure is more complicated than linear and bilinear IFE functions because each function in $\mathcal{P}^k(T), k \geq 2$ has more coefficients so that the jump conditions (1c) and (1d) are not sufficient to determine them. A few explorations for constructing higher degree IFE functions for elliptic interface problems are reported in [1–3, 48]. These research works suggest to add a suitable set of extended jump conditions so that a higher degree IFE shape function can be determined on an interface element. To be specific, we follow [3] to consider the following extended jump conditions:

Normal Extended Jump Conditions

$$\left[\beta \frac{\partial^j u}{\partial \mathbf{n}^j} \right]_\Gamma = 0, \quad j = 2, 3, \ldots k. \tag{8}$$

For each element T in a triangular mesh $\mathcal{T}_h$, we let $\mathcal{I} = \{1, 2, \dots, \frac{(k+1)(k+2)}{2}\}$ be the set of indices of the local nodes $X_{i,T}, i \in \mathcal{I}$ associated with the standard k-th degree Lagrange finite element shape functions $\psi_{j,T}$, $j \in \mathcal{I}$ in T such that

$$\psi_{j,T}(X_{i,T}) = \delta_{ij}, \quad i, j \in \mathcal{I}.$$

When T is an interface element, we let $T^1 = \Omega^1 \cap T$ and $T^2 = \Omega^2 \cap T$, accordingly, we define $\mathcal{I}^1 = \{i \,:\, X_i \in T^1\}$ and $\mathcal{I}^2 = \{i \,:\, X_i \in T^2\}$ so that $\mathcal{I} = \mathcal{I}^1 \cup \mathcal{I}^2$. The k-th degree IFE shape function on this interface element T is a piecewise polynomial in the following form:

$$\phi_{i,T}(x, y) = \begin{cases} \phi^1_{i,T} = \sum\limits_{j \in \mathcal{I}^1} \delta_{ij}\, \psi_{j,T}(x, y) + \sum\limits_{j \in \mathcal{I}^2} c_j\, \psi_{j,T}(x, y) & \text{on } T^1, \\ \phi^2_{i,T} = \sum\limits_{j \in \mathcal{I}^2} \delta_{ij}\, \psi_{j,T}(x, y) + \sum\limits_{j \in \mathcal{I}^1} c_j\, \psi_{j,T}(x, y) & \text{on } T^2. \end{cases} \tag{9}$$

It is easy to see that $\phi_{i,T}(x, y)$ is in the set $\mathcal{P}^k$ and it can be directly verified that

$$\phi_{i,T}(X_{k,T}) = \delta_{ik}, \quad i, k \in \mathcal{I}.$$

Furthermore, it has been proved in [3] that the coefficient $c_j, j \in \mathcal{I}$ can be determined by the interface jump conditions (1c) and (1d) together with the extended jump conditions (8) in a least squares framework such that $\mathbf{c} = (c_j)_{j \in \mathcal{I}}$ is the minimizer of a cost function

$$J(\mathbf{c}) = |\boldsymbol{\eta}^{\mathrm{T}}\mathbf{c} + \boldsymbol{\xi}^{\mathrm{T}}\boldsymbol{v}|_{J_1}, \tag{10}$$

defined for $\phi_{i,T}$ to satisfy interface jump conditions and the extended jump conditions in a weak sense, where $\boldsymbol{v} = (\delta_{ij})_{j \in \mathcal{I}}$, $\boldsymbol{\xi} = (\xi_{j,T})_{j \in \mathcal{I}}$, $\boldsymbol{\eta} = (\eta_{j,T})_{j \in \mathcal{I}}$, with $\xi_{j,T}$ and $\eta_{j,T}$ defined in (2.3) in [3], the semi-norm $|.|_{J_1}$ is defined in (2.12) in [3]. Finally, we define the local k-th degree IFE space on each element $T \in \mathcal{T}_h$ as follows:

$$S_h^k(T) = \begin{cases} \text{Span}\{\psi_{i,T}, i = 1, 2, ..., |\mathcal{I}|\} = \mathbb{P}^k(T), & T \in \mathcal{T}_h^{\mathrm{n}}, \\ \text{Span}\{\phi_{i,T}, i = 1, 2, ..., |\mathcal{I}|\}, & T \in \mathcal{T}_h^{\mathrm{i}}. \end{cases} \tag{11}$$

3 IFE Methods for Helmholtz Interface Problems

Basically, all the IFE methods developed for the elliptic interface problems such as those in [1, 27, 41, 42, 44, 45] can be extended to Helmholtz interface problems. We will focus on the PPIFE method and the DGIFE method because it has been observed that, for the elliptic interface problems, the penalty terms in these methods enhance the stability as well as the accuracy.

The PPIFE method and the DGIFE method use different IFE spaces defined on a mesh $\mathcal{T}_h$. To describe these IFE spaces, we let $\mathcal{N}_h$ be the set of the standard nodes for the Lagrange global finite element basis function, i.e.,

$$\mathcal{N}_h = \begin{cases} \bigcup\limits_{T \in \mathcal{T}_h} \{X_{i,T}, 1 \le i \le (k+1)(k+2)/2\}, & \text{when } \mathcal{T}_h \text{ is a triangular mesh,} \\ \bigcup\limits_{T \in \mathcal{T}_h} \{A_{i,T}, 1 \le i \le 4\}, & \text{when } \mathcal{T}_h \text{ is a rectangular mesh,} \end{cases}$$

where $X_{i,T}, 1 \le i \le (k+1)(k+2)/2$ are the local nodes associated with the standard k-th degree Lagrange finite element shape functions in a triangular element T and $A_{i,T}, 1 \le i \le 4$ are vertices of a rectangular element T. The IFE space for the PPIFE method is defined with the local IFE space on every element as follows:

$$S_h^k(\Omega) = \left\{ v \in L^2(\Omega) \ : \ v|_T \in S_h^k(T), \ \ \forall T \in \mathcal{T}_h, v \text{ is continuous at each } X \in \mathcal{N}_h \right\}. \tag{12}$$

On the other hand, the IFE space for the DGIFE method is defined with the local IFE space on every element without the continuity requirement at nodes of the mesh:

$$DS_h^k(\Omega) = \left\{ v \in L^2(\Omega) \ : \ v|_T \in S_h^k(T), \ \ \forall T \in \mathcal{T}_h \right\}. \tag{13}$$

We note that, according to the mesh, each function $v_h \in S_h^k(\Omega)$ is either a piecewise k-th degree polynomial or a piecewise bilinear polynomial. The continuity of $v_h \in S_h^k(\Omega)$ at every $X \in \mathcal{N}_h$ implies that v_h is continuous across every non-interface edge $e \in \mathring{\mathcal{E}}_h^{\mathrm{n}}$, but, in general, $v_h \in S_h^k(\Omega)$ can be discontinuous across each interface edge $e \in \mathring{\mathcal{E}}_h^{\mathrm{i}}$; see [27, 41] for more related explanations. As usual, each function $v_h \in DS_h^k(\Omega)$ can be discontinuous across all edges of the mesh. Furthermore, for each function $v_h \in S_h^k(\Omega)$ or $DS_h^k(\Omega)$, it can be shown that $v_h|_T \in H^1(T)$ for $k = 1$ because $v_h|_T$ is continuous across $l = \overline{DE}$, see Fig. 1, and $v_h|_T \notin H^1(T)$ for $k \ge 2$ because the piecewise polynomial v_h cannot be continuous across an interface curve Γ in general.

We will also adopt the following standard notations for the penalty terms on edges of a mesh $\mathcal{T}_h$. On each $e \in \mathring{\mathcal{E}}_h$ shared by two elements T_1^e and T_2^e, we let

$$[v]_e = v|_{T_1^e} - v|_{T_2^e}, \quad \text{and} \quad \{v\}_e = \frac{1}{2}(v|_{T_1^e} + v|_{T_2^e}). \tag{14}$$

For $e \in \mathcal{E}_h^b$, we define

$$[v]_e = \{v\}_e = v|_e. \tag{15}$$

Similarly, on the interface $\Gamma \cap T$ inside an interface element T, we let

$$[v]_\Gamma = v|_{T^1} - v|_{T^2}, \quad \text{and} \quad \{v\}_\Gamma = \frac{1}{2}\left(v|_{T^1} + v|_{T^2}\right). \tag{16}$$

3.1 PPIFE Methods for Helmholtz Interface Problems

To derive a PPIFE scheme, multiply Eq. (1a) by the complex conjugate of a function $v_h \in S_h^k(\Omega)$ and integrate on each element $T \in \mathcal{T}_h$. Then, by Green's formula and the interface jump condition (1d), it follows

$$\int_T \beta \nabla u \nabla \overline{v_h} \mathrm{d}X - \int_{\partial T} \beta \nabla u \cdot \boldsymbol{n}_T \overline{v_h} \mathrm{d}s - \int_{\Gamma \cap T} \{\beta \nabla u \cdot \boldsymbol{n}_\Gamma\} [\overline{v_h}] \mathrm{d}s - w^2 \int_T u \overline{v_h} \mathrm{d}X = \int_T f \overline{v_h} \mathrm{d}X, \tag{17}$$

where the third term on the left of (17) disappears when $T \in \mathcal{T}_h^n$. Summing (17) over all $T \in \mathcal{T}_h$ leads to

$$\begin{aligned} &\sum_{T \in \mathcal{T}_h} \int_T \beta \nabla u \nabla \overline{v_h} \mathrm{d}X - \sum_{e \in \mathring{\mathcal{E}}_h} \int_e \{\beta \nabla u \cdot \boldsymbol{n}_e\} [\overline{v_h}] \mathrm{d}s - \sum_{e \in \mathcal{E}_h^{\mathrm{b}}} \int_e \beta \nabla u \cdot \boldsymbol{n}_e \overline{v_h} \mathrm{d}s \\ &- \sum_{T \in \mathcal{T}_h^i} \int_{\Gamma \cap T} \{\beta \nabla u \cdot \boldsymbol{n}_\Gamma\} [\overline{v_h}] \mathrm{d}s - w^2 \int_\Omega u \overline{v_h} \mathrm{d}X = \int_\Omega f \overline{v_h} \mathrm{d}X. \end{aligned} \tag{18}$$

Because of the continuity of $\overline{v_h} \in S_h^k(\Omega)$ across non-interface edges, we can write (18) as

$$\sum_{T\in\mathcal{T}_h}\int_T \beta\nabla u\nabla\overline{v_h}\mathrm{d}X - \sum_{e\in\mathring{\mathcal{E}}_h^{\mathrm{i}}}\int_e \{\beta\nabla u\cdot\boldsymbol{n_e}\}[\overline{v_h}]\mathrm{d}s - \sum_{e\in\mathcal{E}_h^{\mathrm{b}}}\int_e \beta\nabla u\cdot\boldsymbol{n_e}\overline{v_h}\mathrm{d}s$$
$$-\sum_{T\in\mathcal{T}_h^{\mathrm{i}}}\int_{\Gamma\cap T}\{\beta\nabla u\cdot\boldsymbol{n_\Gamma}\}[\overline{v_h}]\mathrm{d}s - w^2\int_\Omega u\overline{v_h}\mathrm{d}X = \int_\Omega f\overline{v_h}\mathrm{d}X.$$

Applying the boundary condition (1b), we can reduce the above equation to

$$\begin{aligned}\sum_{T\in\mathcal{T}_h}\int_T \beta\nabla u\nabla\overline{v_h}\mathrm{d}X - \sum_{e\in\mathring{\mathcal{E}}_h^{\mathrm{i}}}\int_e \{\beta\nabla u\cdot\boldsymbol{n_e}\}[\overline{v_h}]\mathrm{d}s + \mathrm{i}w\sum_{e\in\mathcal{E}_h^{\mathrm{b}}}\int_e u\overline{v_h}\mathrm{d}s\\ -\sum_{T\in\mathcal{T}_h^{\mathrm{i}}}\int_{\Gamma}\{\beta\nabla u\cdot\boldsymbol{n_\Gamma}\}[\overline{v_h}]\mathrm{d}s - w^2\int_\Omega u\overline{v_h}\mathrm{d}X = \int_\Omega f\overline{v_h}\mathrm{d}X + \sum_{e\in\mathcal{E}_h^{\mathrm{b}}}\int_e g\overline{v_h}\mathrm{d}s,\end{aligned} \tag{19}$$

By assuming that u is in $PH^2(\Omega)$ so that $[u]_e = 0,\ \forall e \in \mathring{\mathcal{E}}_h$ and applying the interface jump condition (1c), we have

$$\begin{aligned}\epsilon\sum_{e\in\mathring{\mathcal{E}}_h^{\mathrm{i}}}\int_e\{\beta\nabla\overline{v_h}\cdot\mathbf{n}_e\}_e[u]_e\mathrm{d}s = 0,\quad \mathrm{i}\sum_{e\in\mathring{\mathcal{E}}_h^{\mathrm{i}}}\frac{\sigma_e^0}{|e|}\int_e[u]_e\,[\overline{v_h}]_e\mathrm{d}s = 0,\\ \epsilon\sum_{T\in\mathcal{T}_h^{\mathrm{i}}}\int_{\Gamma\cap T}\{\beta\nabla\overline{v_h}\cdot\mathbf{n}_\Gamma\}_\Gamma[u]_\Gamma\mathrm{d}s = 0,\quad \mathrm{i}\sum_{T\in\mathcal{T}_h^{\mathrm{i}}}\frac{\sigma_e^0}{|e|}\int_{\Gamma\cap T}[u]_\Gamma\,[\overline{v_h}]_\Gamma\mathrm{d}s = 0,\end{aligned} \tag{20}$$

with parameters ϵ, and $\sigma_e^0 \geq 0$. Adding these four terms to (19), we can see that the solution u to the Helmholtz interface problem (1) satisfies the following form:

$$a_h^{PP}(u, v_h) - w^2(u, v_h)_{L^2(\Omega)} = L_f(v_h),\quad \forall v_h \in S_h^k(\Omega), \tag{21}$$

where the bilinear form $a_h^{PP}(\cdot,\cdot) : PH^2(\Omega)\times S_h^k(\Omega)\to\mathbb{R}$ is defined as

$$\begin{aligned}a_h^{PP}(u, v_h) = \sum_{T\in\mathcal{T}_h}\int_T\beta\nabla u\cdot\nabla\overline{v_h}\mathrm{d}X - \sum_{e\in\mathring{\mathcal{E}}_h^{\mathrm{i}}}\int_e\{\beta\nabla u\cdot\mathbf{n}_e\}_e[\overline{v_h}]_e\mathrm{d}s + \epsilon\sum_{e\in\mathring{\mathcal{E}}_h^{\mathrm{i}}}\int_e\{\beta\nabla\overline{v_h}\cdot\mathbf{n}_e\}_e[u]_e\mathrm{d}s\\ + \mathrm{i}w\sum_{e\in\mathcal{E}_h^{\mathrm{b}}}\int_e u\overline{v_h}\mathrm{d}s + \mathrm{i}\sum_{e\in\mathring{\mathcal{E}}_h^{\mathrm{i}}}\frac{\sigma_e^0}{|e|}\int_e[u]_e\,[\overline{v_h}]_e\mathrm{d}s - \sum_{T\in\mathcal{T}_h^{\mathrm{i}}}\int_{\Gamma\cap T}\{\beta\nabla u\cdot\mathbf{n}_\Gamma\}[\overline{v_h}]_\Gamma\mathrm{d}s\\ + \epsilon\sum_{T\in\mathcal{T}_h^{\mathrm{i}}}\int_{\Gamma\cap T}\{\beta\nabla\overline{v_h}\cdot\mathbf{n}_\Gamma\}_\Gamma[u]_\Gamma\mathrm{d}s + \mathrm{i}\sum_{T\in\mathcal{T}_h^{\mathrm{i}}}\frac{\sigma_e^0}{|e|}\int_{\Gamma\cap T}[u]_\Gamma\,[\overline{v_h}]_\Gamma\mathrm{d}s,\end{aligned} \tag{22}$$

and the linear form $L_f(\cdot) : S_h^k(\Omega)\to\mathbb{R}$ is defined as

$$L_f(v_h) = \int_\Omega f\overline{v_h}\mathrm{d}X + \sum_{e\in\mathcal{E}_h^b}\int_e g\overline{v_h}\mathrm{d}s. \tag{23}$$

The weak form (21) suggests the PPIFE method for the Helmholtz interface problem (1): find $u_h \in S_h^k(\Omega)$, $k \geq 1$ such that

$$a_h^{PP}(u_h, v_h) - w^2(u_h, v_h)_\Omega = L_f(v_h), \quad \forall v_h \in S_h^k(\Omega). \tag{24}$$

Remark 3.1 The continuity of $v_h|T$, $\forall T \in \mathcal{T}_h$ for every $v_h \in S_h^1(\Omega)$ implies that the last three terms in the bilinear form $a_h^{PP}(\cdot,\cdot)$ defined in (22) can be ignored in the PPIFE method based on the linear and bilinear IFE spaces.

3.2 DGIFE Method for Helmholtz Interface Problems

For the DGIFE method, instead of using $v_h \in S_h^k(\Omega)$, by using $v_h \in DS_h^k(\Omega)$ in (18) and then adding those four terms in (20), we can see that the solution u to the Helmholtz interface problem (1) satisfies the following form:

$$a_h^{\mathrm{DG}}(u, v_h) - w^2(u, v_h)_\Omega = L_f(v_h), \quad \forall v_h \in DS_h^k(\Omega), \tag{25}$$

where the bilinear form $a_h^{\mathrm{DG}}(\cdot,\cdot) : PH^2(\Omega) \times DS_h^k(\Omega) \to \mathbb{R}$ is defined by

$$\begin{aligned} a_h^{\mathrm{DG}}(u, v_h) = & \sum_{T\in\mathcal{T}_h} \int_T \beta \nabla u \cdot \nabla \overline{v_h} \mathrm{d}X - \sum_{e\in\mathring{\mathcal{E}}_h} \int_e \{\beta \nabla u \cdot \mathbf{n}_e\}_e [\overline{v_h}]_e \mathrm{d}s + \epsilon \sum_{e\in\mathring{\mathcal{E}}_h} \int_e \{\beta \nabla \overline{v_h} \cdot \mathbf{n}_e\}_e [u]_e \mathrm{d}s \\ & + \mathrm{i}w \sum_{e\in\mathcal{E}_h^{\mathrm{b}}} \int_e u \overline{v_h} \mathrm{d}s + \mathrm{i} \sum_{e\in\mathring{\mathcal{E}}_h} \frac{\sigma_e^0}{|e|} \int_e [u]_e \, [\overline{v_h}]_e \mathrm{d}s - \int_\Gamma \{\beta \nabla u \cdot \boldsymbol{n}_\Gamma\} [\overline{v_h}]_\Gamma \mathrm{d}s \\ & + \epsilon \int_\Gamma \{\beta \nabla \overline{v_h} \cdot \mathbf{n}_\Gamma\}_\Gamma [u]_\Gamma \mathrm{d}s + \mathrm{i} \frac{\sigma_e^0}{|e|} \int_\Gamma [u]_\Gamma \, [\overline{v_h}]_\Gamma \mathrm{d}s, \end{aligned} \tag{26}$$

and the linear functional $L_f(\cdot) : DS_h^k(\Omega) \to \mathbb{R}$ has the same form as (23). The weak form (25) suggests the DGIFE method for the Helmholtz interface problem: find $u_h \in DS_h^k(\Omega)$, $k \geq 1$ such that

$$a_h^{\mathrm{DG}}(u_h, v_h) - w^2(u_h, v_h)_\Omega = L_f(v_h), \quad \forall v_h \in DS_h^k(\Omega). \tag{27}$$

Remark 3.2 Similar to the PPIFE method, the continuity of $v_h|T$, $\forall T \in \mathcal{T}_h$ for every $v_h \in DS_h^1(\Omega)$ implies that the last three terms in the bilinear form $a_h^{\mathrm{DG}}(\cdot,\cdot)$ defined in (26) can be ignored in the DGIFE method based on the linear and bilinear IFE spaces.

4 Numerical Examples

We now present a few numerical examples to illustrate features of IFE methods for the Helmholtz interface problems. In these numerical examples, the solution domain is $\Omega = (-1, 1) \times (-1, 1)$ on which we form a rectangular mesh $\mathcal{T}_h$ by partitioning Ω into $N \times N$ congruent squares of size $h = 2/N$ or we construct a Cartesian triangular mesh $\mathcal{T}_h$ by further dividing each rectangular element in the previous rectangular mesh into two congruent triangles along its diagonal line. The Helmholtz interface problem to be considered is such that it has an interface $\Gamma : x^2 + y^2 - r_0^2 = 0, r_0 = \pi/6.28$ separating Ω into two subdomains

$$\Omega^1 = \{(x, y) : x^2 + y^2 < r_0^2\}, \quad \Omega^2 = \Omega \backslash \overline{\Omega^1}.$$

Functions f and g in the Helmholtz interface problem (1) are chosen such that its exact solution is

$$u(x, y) = \begin{cases} \dfrac{1}{\beta_1} U(r), & (x, y) \in \Omega^1, \\ \dfrac{1}{\beta_2} U(r) + \left(\dfrac{1}{\beta_1} - \dfrac{1}{\beta_2} \right) U(r_0), & (x, y) \in \Omega^2, \end{cases} \tag{28}$$

where $r = \sqrt{x^2 + y^2}$, $U(r) = \frac{\cos(wr)}{w} - \frac{\cos(w)+\mathrm{i}\sin(w)}{w(\mathrm{J}_0(w)+\mathrm{i}\mathrm{J}_1(w))}\mathrm{J}_0(wr)$, and $\mathrm{J}_\gamma(z), \gamma = 0, 1$ are the 0-th and 1-st order Bessel functions of the first kind.

For the PPIFE and DGIFE scheme, we choose $\epsilon = -1$, so the PPIFE and DGIFE schemes are symmetric PPIFE (SPPIFE)/symmetric DGIFE (SDGIFE) schemes, respectively, and we choose the penalty parameter $\sigma_e^0 = 30\max\{\beta_1, \beta_2\}$. We apply these IFE methods to Helmholtz interface problems with $\beta_1 = 1$, $\beta_2 = 5$ or 50 representing small and moderately large discontinuity in the coefficient β, and to Helmholtz interface problems with $w = 10$ or 50 for small and larger wave numbers.

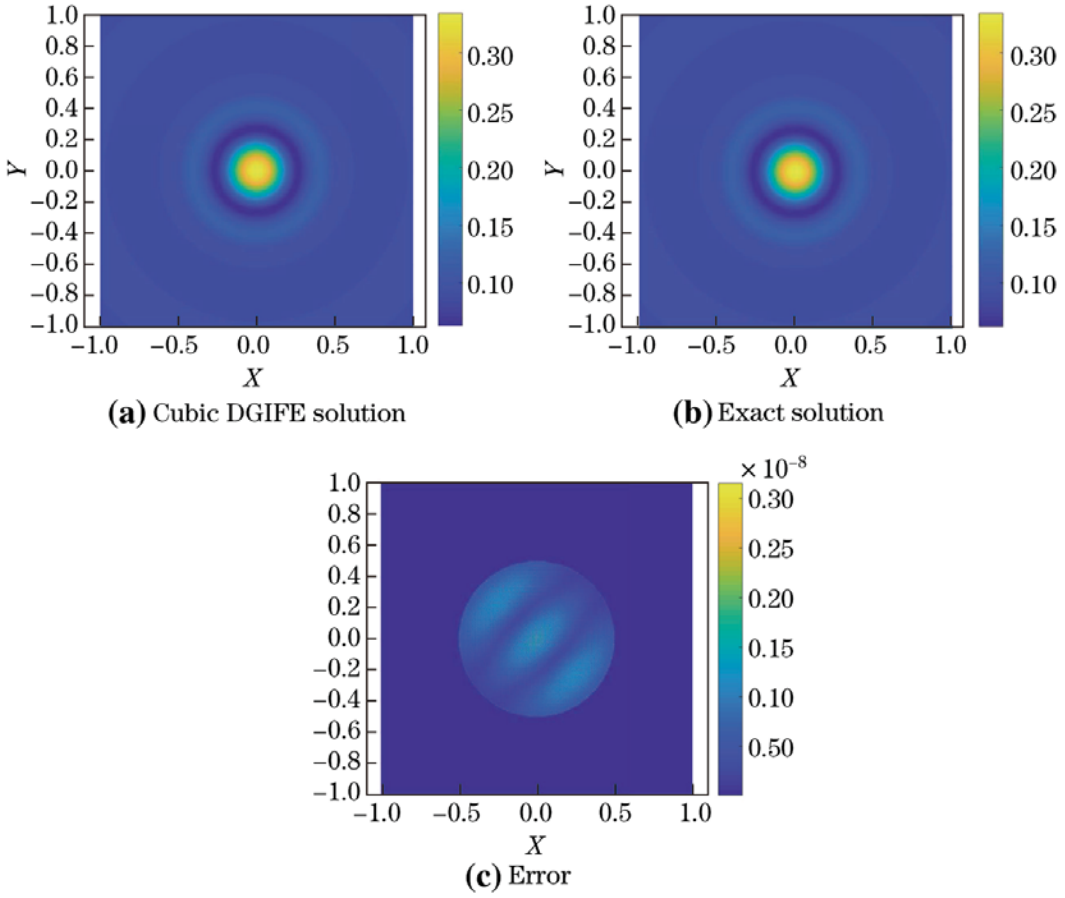

Fig. 2 Magnitude of cubic DGIFE solution, exact solution and errors between them at finite element nodes when $w = 10$, $\beta_1 = 1$, $\beta_2 = 50$, $N = 160$

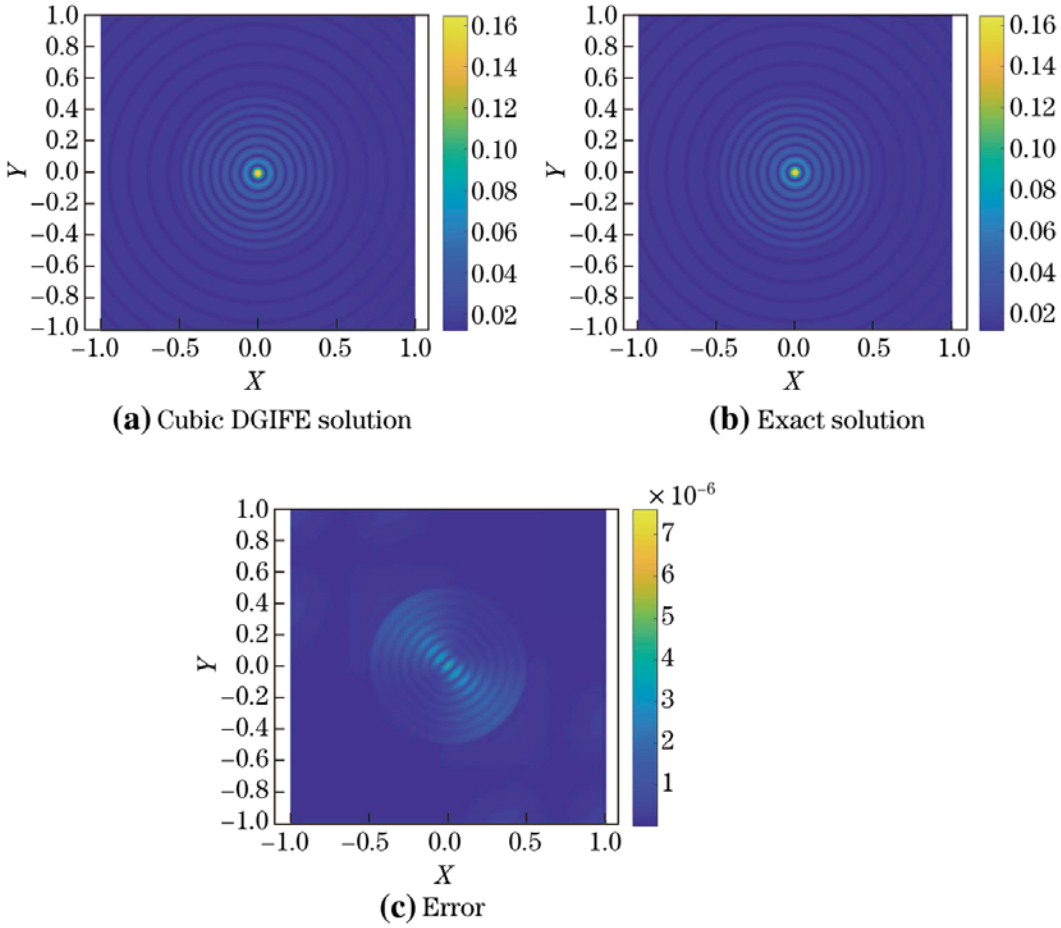

Fig. 3 Magnitude of cubic DGIFE solution, exact solution and errors between them at finite element nodes when $w = 50$, $\beta_1 = 1$, $\beta_2 = 50$, $N = 160$

Figures 2, 3, 4 and 5 compare the cubic DGIFE solutions to the exact solutions of two groups of Helmholtz interface problems. Figures 2 and 3 are for the interface problems whose coefficient β is such that $\beta_1 = 1, \beta_2 = 50$, but Figs. 4 and 5 are for $\beta_1 = 50, \beta_2 = 1$. These plots demonstrate that the proposed IFE methods can satisfactorily solve the Helmholtz interface problems with either a small wave number $w = 10$ or a moderately large wave number $w = 50$.

From Figs. 2, 3, 4 and 5, we also observe that the solution u oscillates more for the Helmholtz interface problem with a larger wave number, and u has a smaller magnitude in the subdomain where β has a larger value. It is well known that the oscillation in the exact solution u in the Helmholtz equation dictates the mesh size for its numerical solution; otherwise, the accuracy or convergence of the numerical solution cannot be guaranteed if the mesh size is not sufficiently small to resolve the oscillation. For the convergence, we recall the critical mesh size discussed in [24] that indicates when the numerical solutions start to converge:

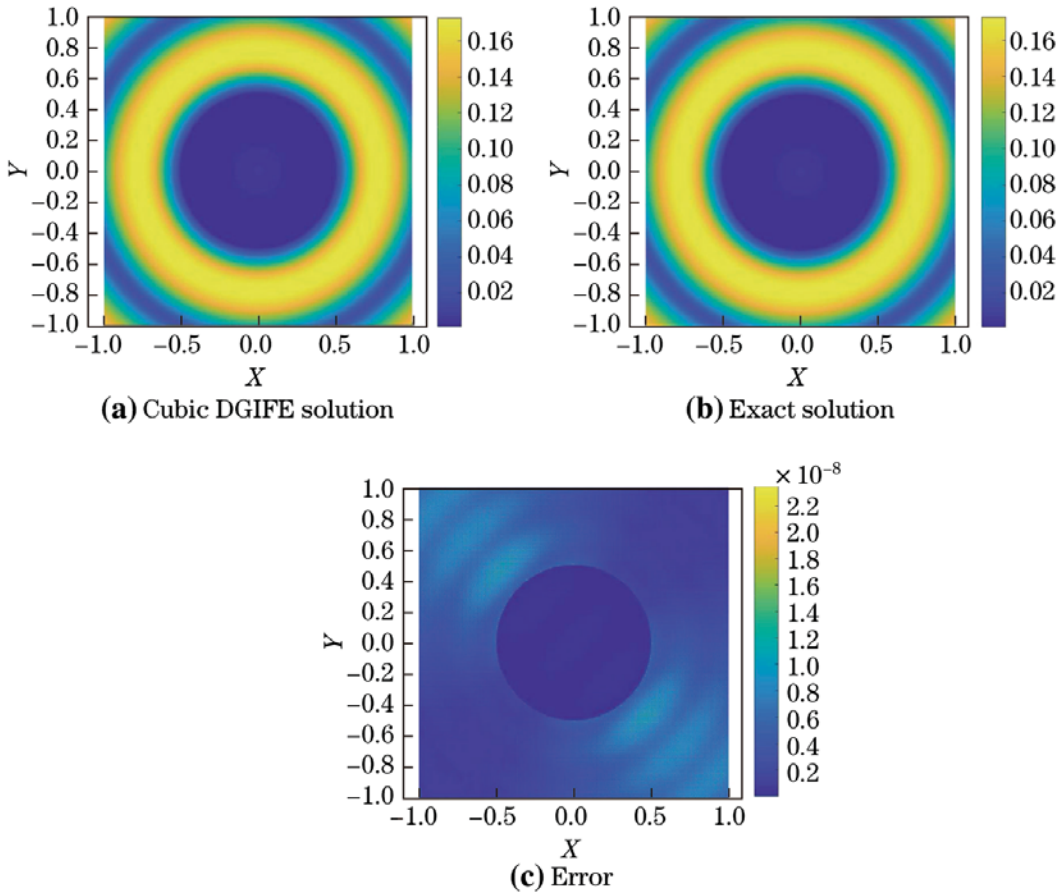

Fig. 4 Magnitude of cubic DGIFE solution, exact solution and errors between them at finite element nodes when $w = 10$, $\beta_1 = 50$, $\beta_2 = 1$, $N = 160$

Definition 4.1 (Critical mesh size) For fixed w and f, the critical mesh size is defined to be the maximum mesh size $H(w, f)$ such that

(C1) $e(h, w) < 1$ for $h < H(w,f)$,
(C2) $e(h, w) \to 0$ as $h \to 0$, where $e(h, w) = |u - u_h|_{1,\Omega}/|u|_{1,\Omega}$ is the relative error in the semi-H^1 norm.

By the data in Table 1, we can see that the linear PPIFE solution converges from a coarse mesh with $h = 2/10$ when the wave number in the interface problem is small $w = 10$, and this suggests the critical mesh size $H(10,f) \lessapprox 2/10$. However, for the interface problem with a large wave number $w = 50$ but a small discontinuity in β, the critical mesh size for the PPIFE solution seems to be much smaller $H(50,f) \lessapprox 2/170$. When the discontinuity in β is larger, the critical mesh size for the linear IFE solution $H(50,f) \lessapprox 2/230$ which is even smaller. Even though not presented here for the sake of controlling the page consumption, we have observed in our numerical experiments that, for either small or large discontinuity in β, the critical mesh size for the cubic PPIFE solution is about 2/10 when the wave number is small $w = 10$, but for a large wave number $w = 50$ it becomes about 2/30. Therefore, higher degree IFE methods can start to converge on rather coarse mesh even for higher wave numbers. Similar behaviors are also observed for the DGIFE solutions.

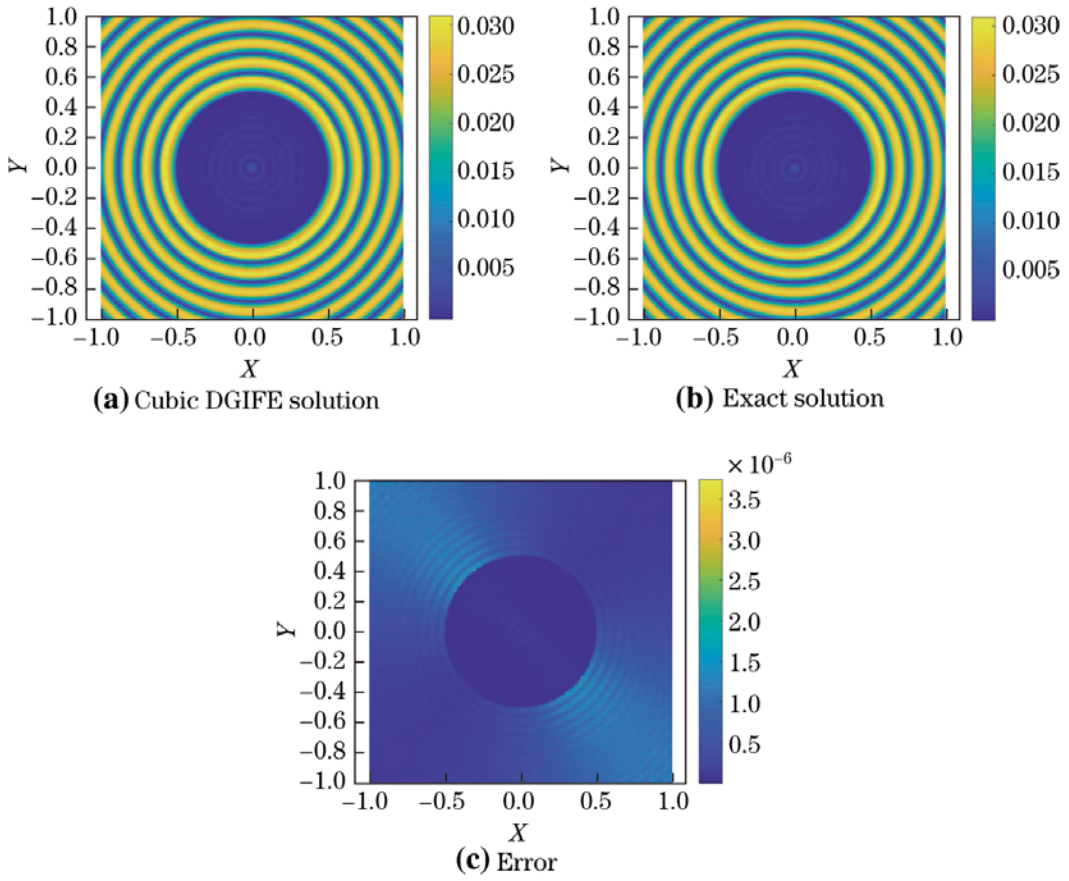

Fig. 5 Magnitude of cubic DGIFE solution, exact solution and errors between them at finite element nodes when $w = 50$, $\beta_1 = 50$, $\beta_2 = 1$, $N = 160$

From the data in Table 1, we can see that IFE solutions do not converge optimally until the mesh is further reduced beyond the critical mesh size, and this motivates us to introduce the optimal mesh size to characterize this phenomenon:

Definition 4.2 (Optimal mesh size) For fixed w and f, the optimal mesh size is defined to be the maximum mesh size $\tilde{H}(w,f)$ such that

(O1) $\|u - u_h\|_{0,\Omega} \approx Ch^{k+1}$ for $h < \tilde{H}(w,f)$,
(O2) $|u - u_h|_{1,\Omega} \approx Ch^k$ for $h < \tilde{H}(w,f)$,

where $k \geq 1$ is the degree of polynomials used in $S_h^k(\Omega)$ and $DS_h^k(\Omega)$.

From the data presented in Tables 1 and 2, we can see that when the wave number is small $w = 10$ and the discontinuity in β is small, the optimal mesh size for the linear PPIFE solution seems to be $\tilde{H}(10,f) \lessapprox 2/360$. But when the discontinuity in β is larger, the optimal mesh size for the linear PPIFE solution seems to be a little smaller $\tilde{H}(10,f) \lessapprox 2/420$. However, for a larger number $w = 50$, the data in Table 1 indicate that the optimal mesh size for the linear PPIFE solution seems to be drastically smaller such that $\tilde{H}(50,f) \lessapprox 2/1280$, and we note that $\tilde{H}(50,f) \ll H(50,f)$, i.e., the optimal mesh size for the linear PPIFE solution is much smaller than its critical mesh size. Similar characteristics is observed for bilinear PPIFE solution, linear DGIFE solution, and bilinear

Table 1 Errors in linear SPPIFE solution and convergence rates for $\beta_1 = 1$, different β_2 and w

w	β_2	N	$\|u - u_h\|_{0,\Omega}$	Rate	$\|u - u_h\|_{1,\Omega}$	Rate	$e(h, w)$
10	5	10	8.2104E−02	NA	7.4639E−01	NA	7.2748E−01
		20	4.9816E−02	0.7208	4.7736E−01	0.6448	4.6526E−01
		40	1.6991E−02	1.5519	2.0544E−01	1.2164	2.0023E−01
		80	4.5312E−03	1.9068	8.7699E−02	1.2281	8.5477E−02
		160	1.1495E−03	1.9789	4.1293E−02	1.0867	4.0247E−02
		320	2.8953E−04	1.9892	2.0298E−02	1.0245	1.9784E−02
		640	7.2356E−05	2.0005	1.0106E−02	1.0062	9.8499E−03
		1280	1.8062E−05	2.0021	5.0476E−03	1.0015	4.9197E−03
10	50	10	6.4644E−02	NA	7.5030E−01	NA	7.5659E−01
		20	3.3762E−02	0.9371	4.0855E−01	0.8769	4.1197E−01
		40	2.0716E−02	0.7047	2.4551E−01	0.7347	2.4756E−01
		80	1.0567E−02	0.9712	1.2749E−01	0.9454	1.2856E−01
		160	3.4762E−03	1.6039	5.1411E−02	1.3102	5.1841E−02
		320	9.1923E−04	1.9190	2.1448E−02	1.2612	2.1627E−02
		640	2.3301E−04	1.9800	1.0022E−02	1.0976	1.0106E−02
		1280	5.8619E−05	1.9910	4.9165E−03	1.0275	4.9576E−03
50	5	80	3.9451E−02	− 0.3967	1.6817E+00	− 0.3401	1.4876E+00
		160	2.8478E−02	0.4702	1.1843E+00	0.5059	1.0357E+00
		170	2.5688E−02	1.7007	1.0693E+00	1.6846	9.4531E−01
		180	2.2661E−02	2.1937	9.4548E−01	2.1536	8.3582E−01
		190	1.9804E−02	2.4923	8.2939E−01	2.4231	7.3319E−01
		200	1.7282E−02	2.6557	7.2717E−01	2.5642	6.4283E−01
		320	5.1669E−03	2.5689	2.3826E−01	2.3740	2.1095E−01
		640	1.2047E−03	2.1006	7.5049E−02	1.6666	6.6484E−02
		1280	2.7773E−04	2.1170	3.0119E−02	1.3171	2.6673E−02
		2560	6.8813E−05	2.0129	1.4235E−02	1.0813	1.2664E−02
50	50	160	4.0513E−02	0.0049	1.8752E+00	0.0178	1.7055E+00
		210	3.3354E−02	0.7150	1.5637E+00	0.6680	1.4222E+00
		220	2.7486E−02	4.1599	1.2931E+00	4.0842	1.1761E+00
		230	2.2856E−02	4.1500	1.0792E+00	4.0680	9.8156E−01
		240	1.9322E−02	3.9462	9.1595E−01	3.8543	8.3306E−01
		250	1.6556E−02	3.7845	7.8804E−01	3.6846	7.1673E−01
		320	7.5321E−03	3.1904	3.7059E−01	3.0562	3.3705E−01
		640	1.4355E−03	2.3915	8.6787E−02	2.0943	7.8931E−02
		1280	3.3874E−04	2.0833	3.1457E−02	1.4641	2.8610E−02
		2560	8.3515E−05	2.0201	1.4101E−02	1.1576	1.2825E−02

DGIFE solution, and this strongly demonstrates the inefficiency of using the lower degree method to solve a Helmholtz interface problem with a large wave number.

On the other hand, for this Helmholtz interface problem with a small wave number $w = 10$, the data in Table 3 show that the optimal mesh size for the cubic PPIFE solution seems to be such that $\tilde{H}(10, f) \lessapprox 2/40$ when β has a small discontinuity, and $\tilde{H}(10, f) \lessapprox 2/80$ when β has a larger discontinuity. For a large wave number $w = 50$, the data in Table 3 show that the optimal mesh size for the cubic PPIFE solution seems

Table 2 Errors in linear SPPIFE solution and convergence rates for $\beta_1 = 1$, different β_2 and w

w	β_2	N	$\|u - u_h\|_{0,\Omega}$	Rate	$\|u - u_h\|_{1,\Omega}$	Rate	$e(h, w)$
10	5	320	2.8953E−04	NA	2.0298E−02	NA	1.9784E−02
		330	2.7060E−04	2.1969	1.9676E−02	1.0115	1.9178E−02
		340	2.5617E−04	1.8364	1.9092E−02	1.0099	1.8608E−02
		350	2.4053E−04	2.1725	1.8540E−02	1.0115	1.8070E−02
		360	2.2829E−04	1.8539	1.8022E−02	1.0064	1.7565E−02
		370	2.1555E−04	2.0964	1.7529E−02	1.0129	1.7084E−02
		380	2.0469E−04	1.9384	1.7066E−02	1.0037	1.6633E−02
		390	1.9430E−04	2.0050	1.6622E−02	1.0129	1.6201E−02
		400	2.0469E−04	2.0265	1.6206E−02	1.0029	1.5795E−02
		410	1.9430E−04	1.9657	1.5806E−02	1.0114	1.5405E−02
10	50	400	5.9551E−04	NA	1.5353E−02	NA	1.6780E−02
		420	5.4036E−04	1.9919	1.5761E−02	1.1128	1.5893E−02
		440	4.9144E−04	2.0400	1.4969E−02	1.1085	1.5094E−02
		460	4.5041E−04	1.9613	1.4260E−02	1.0924	1.4379E−02
		480	4.1440E−04	1.9577	1.4260E−02	1.0840	1.3731E−02
		500	3.8156E−04	2.0225	1.3617E−02	1.0848	1.3136E−02
		520	3.5217E−04	2.0434	1.3027E−02	1.0795	1.2591E−02
		540	3.2554E−04	2.0840	1.1996E−02	1.0773	1.2090E−02
		560	2.8306E−04	1.9568	1.1538E−02	1.0611	1.1207E−02
		580	2.6451E−04	1.9994	1.1118E−02	1.0574	1.0812E−02

to be such that $\tilde{H}(50,f) \lessapprox 2/260$ which is much larger than the optimal mesh size for the linear PPIFE solution. Therefore, the higher degree IFE methods are advantageous because they can converge optimally on much coarser mesh than lower degree PPIFE methods. Similar behavior has also been observed for DGIFE methods in our numerical experiments.

We can also see the advantage of higher degree IFE methods from the point of view of the global degrees of freedom and accuracy. According to the discussions above, for a small wave number $w = 10$ and a small discontinuity in β, the linear PPIFE solution starts to converge optimally once its mesh size is such that $h = \tilde{H}(10,f) \lessapprox 2/360$, and on such a mesh, the global degrees of freedom (GDOF) in this linear PPIFE solution is about $(361)^2 = 130321$. In comparison, the cubic PPIFE solution starts to converge optimally once its mesh size is such that $h = \tilde{H}(10,f) \lessapprox 2/40$, and the GDOF in this cubic PPIFE solution is about $(3 \times 40 + 1)^2 = 14641$ which is about 9 times smaller than the GDOF of the linear PPIFE solution. Far more importantly, by comparing data in Tables 1, 2, and 3, we can see that, on meshes whose mesh sizes are smaller than the optimal mesh sizes, the cubic PPIFE solution is obviously far more accurate than the linear PPIFE solution even though the GDOF of the linear PPIFE solution is much larger. Similar advantages are also observed for higher degree DGIFE methods. Therefore, for wave propagation interface problems, the higher degree IFE methods should be preferred even though the development of higher degree IFE methods is still in its early stage, and its research deserves more attention.

By design, the linear and bilinear IFE spaces are consistent with their corresponding FE spaces, i.e., the linear/bilinear IFE space becomes linear/bilinear FE space when

Table 3 Errors in cubic SPPIFE solution and convergence rates for $\beta_1 = 1$, different β_2 and w

w	β_2	N	$\|u - u_h\|_{0,\Omega}$	Rate	$\|u - u_h\|_{1,\Omega}$	Rate	$e(h, w)$
10	5	40	1.7107E−06	NA	4.1486E−04	NA	4.1486E−04
		50	6.9536E−07	4.0343	2.1274E−04	2.9930	2.1274E−04
		60	3.3424E−07	4.0180	1.2326E−04	2.9937	1.2326E−04
		70	1.7995E−07	4.0168	7.7668E−05	2.9960	7.7668E−05
		80	1.0543E−07	4.0033	5.2073E−05	2.9941	5.2073E−05
10	50	80	1.0522E−07	NA	5.1511E−05	NA	5.1942E−05
		90	6.5444E−08	4.0319	3.6176E−05	3.0005	3.6478E−05
		100	4.2864E−08	4.0164	2.6386E−05	2.9950	2.6607E−05
		110	2.9224E−08	4.0187	1.9829E−05	2.9973	1.9995E−05
		120	2.0628E−08	4.0033	1.5276E−05	2.9982	1.5404E−05
		130	1.4951E−08	4.0218	1.2009E−05	3.0060	1.2110E−05
50	5	160	1.0869E−06	4.3450	9.8166E−04	2.9970	8.6781E−04
		180	6.5893E−07	4.2427	6.8980E−04	2.9983	6.0979E−04
		200	4.2458E−07	4.1736	5.0307E−04	2.9978	4.4472E−04
		220	2.8662E−07	4.1252	3.7808E−04	2.9972	3.3423E−04
		240	2.0079E−07	4.0882	2.9128E−04	2.9976	2.5750E−04
		260	1.4498E−07	4.0646	2.2913E−04	2.9993	2.0256E−04
		280	1.0736E−07	4.0497	1.8349E−04	3.0001	1.6220E−04
		300	8.1240E−08	4.0363	1.4921E−04	2.9984	1.3190E−04
		320	6.2625E−08	4.0245	1.2296E−04	2.9963	1.0870E−04
50	50	160	1.0830E−06	4.4365	9.4940E−04	2.9972	8.6348E−04
		180	6.5049E−07	4.3017	6.6717E−04	2.9970	6.0680E−04
		200	4.1663E−07	4.2111	4.8660E−04	2.9963	4.4257E−04
		220	2.8016E−07	4.1513	3.6573E−04	2.9960	3.3263E−04
		240	1.9577E−07	4.1099	2.8179E−04	2.9962	2.5629E−04
		260	1.4112E−07	4.0807	2.2170E−04	2.9956	2.0164E−04
		280	1.0438E−07	4.0646	1.7754E−04	2.9965	1.6147E−04
		300	7.8916E−08	4.0491	1.4437E−04	2.9958	1.3131E−04
		320	6.0794E−08	4.0364	1.1898E−04	2.9948	1.0821E−04

$\beta_1 = \beta_2$. Additionally, the formulations for the PPIFE method and the FE method are quite close to each other, and they differ only on interface elements whose union forms a small band around the interface. Therefore, it is interesting to know how the PPIFE and FE solutions behave from the point of views of the critical mesh size and the optimal mesh size. From the data in Table 4, when the wave number is small $w = 10$, the critical mesh size for the linear FE solution is about 2 / 10 which is not much different from the critical mesh size for the linear IFE solution according to the data in Table 1. For a larger wave number $w = 50$, the data in Table 4 indicate that the critical mesh size for the linear FE solution is about 2 / 140 which is again not much different from the critical mesh size for the linear IFE solution which is about 2 / 170 when the discontinuity in β is small according to the data in Table 1, but the difference becomes a little more obvious when the discontinuity is larger. We also have observed that the critical mesh size of a cubic IFE method is just slightly smaller than that of its FE counterpart. As for the optimal mesh size, by Table 4, when the wave number is small $w = 10$, the optimal mesh size for the linear FE solution

Table 4 Errors in linear FE solution for $\beta_1 = \beta_2 = 1$

w	β_2	N	$\|u - u_h\|_{0,\Omega}$	Rate	$\|u - u_h\|_{1,\Omega}$	Rate	$e(h, w)$
10	1	10	1.4494E−01	NA	1.5230E+00	NA	9.2162E−01
		20	6.4454E−02	1.1692	7.9105E−01	0.9450	4.7870E−01
		40	1.8912E−02	1.8572	3.1627E−01	1.3221	1.9139E−01
		80	4.9128E−03	1.9713	1.3738E−01	1.1335	8.3135E−02
		90	3.8919E−03	1.9778	1.2056E−01	1.1089	7.2956E−02
		100	3.1583E−03	1.9823	1.0748E−01	1.0901	6.5040E−02
		110	2.6138E−03	1.9856	9.7007E−02	1.0755	5.8703E−02
50	1	80	4.2659E−02	NA	2.1287E+00	NA	1.2300E+00
		90	4.1340E−02	0.2668	2.0649E+00	0.2584	1.1931E+00
		100	4.0504E−02	0.1937	2.0246E+00	0.1874	1.1698E+00
		110	3.9731E−02	0.2023	1.9877E+00	0.1929	1.1485E+00
		120	3.8340E−02	0.4094	1.9218E+00	0.3876	1.1104E+00
		130	3.6248E−02	0.7011	1.8218E+00	0.6671	1.0527E+00
		140	3.3800E−02	0.9438	1.7040E+00	0.9021	9.8458E−01
		150	3.1281E−02	1.1224	1.5821E+00	1.0758	9.1415E−01
		160	2.8836E−02	1.2611	1.4632E+00	1.2106	8.4544E−01

Table 5 Errors in cubic FE solution for $\beta_1 = \beta_2 = 1$

w	β_2	N	$\|u - u_h\|_{0,\Omega}$	Rate	$\|u - u_h\|_{1,\Omega}$	Rate	$e(h, w)$
50	1	240	3.1879E−07	4.1290	4.6238E−04	2.9985	2.6717E−04
		250	2.6955E−07	4.1100	4.0911E−04	2.9986	2.3638E−04
		260	2.2952E−07	4.0982	3.6372E−04	2.9987	2.1016E−04
		270	1.9674E−07	4.0840	3.2480E−04	2.9987	1.8767E−04
		280	1.6963E−0	4.0763	2.9124E−04	2.9989	1.6828E−04
		290	1.4708E−07	4.0655	2.6215E−04	2.9989	1.5147E−04
		300	1.2816E−07	4.0607	2.3680E−04	2.9990	1.3683E−04
		310	1.1222E−07	4.0518	2.1463E−04	2.9990	1.2401E−04
		320	9.8681E−08	4.0491	1.9513E−04	2.9991	1.1275E−04

seems to be about 2 / 100 which is obviously larger than the optimal mesh for the linear PPIFE solution which is about 2 / 360 when the discontinuity in β is small. However, for a large wave number $w = 50$, the data in Table 5 suggest that the optimal mesh for the cubic FE solution is about 2 / 260 which is comparable to the optimal mesh size for the cubic PPIFE solution suggested by the data in Table 3. Similar behaviors are also observed for DGIFE and DG methods. In summary, for Helmholtz problems, higher degree IFE methods and FE methods behave somewhat similarly, especially when the discontinuity in β is small or from the point of view of the optimal mesh size.

5 Conclusions

We consider two IFE methods: the PPIFE and DGIFE methods for solving the Helmholtz interface problem. For the Helmholtz interface problem with a small wave number, the proposed PPIFE and DGIFE methods can produce optimally convergent approximate solutions on interface-independent meshes whose mesh size is fine enough. However, when the wave number is large, the lower degree (linear or bilinear) IFE methods do not seem to be good choices because they usually do not demonstrate the optimal convergence unless the mesh size is extremely small. Instead, our explorations strongly suggest to use higher degree IFE methods because they can quickly start to converge optimally and produce far more accurate numerical solutions when the mesh size is reduced. Numerical experiments demonstrate that a large discontinuity in the coefficient β will challenge the PPIFE and DGIFE methods, but this kind of challenge seems to be at a level far lower than the challenge from a large wave number. We also have observed that higher degree IFE methods and higher degree FE methods behave somewhat similarly from the point of view of the *critical mesh size* and the *optimal mesh size*.

Acknowledgements This research was partially supported by GRF B-Q56D of HKSAR and Polyu G-UA7V.

References

1. Adjerid, S., Ben-Romdhane, M., Lin, T.: Higher degree immersed finite element methods for second-order elliptic interface problems. Int. J. Numer. Anal. Model. **11**(3), 541–566 (2014)
2. Adjerid, S., Ben-Romdhane, M., Lin, T.: Higher degree immersed finite element spaces constructed according to the actual interface. Comput. Math. Appl. **75**(6), 1868–1881 (2018)
3. Adjerid, S., Guo, R., Lin, T.: High degree immersed finite element spaces by a least squares method. Int. J. Numer. Anal. Model. **14**(4/5), 604–626 (2017)
4. Ainsworth, M.: Dispersive and dissipative behaviour of high order discontinuous Galerkin finite element methods. J. Comput. Phys. **198**, 106–130 (2004)
5. Annavarapu, C., Hautefeuille, M., Dolbow, J.: A finite element method for crack growth without remeshing. Comput. Methods Appl. Mech. Eng. **225–228**, 44–54 (2012)
6. Aziz, A.K., Werschulz, A.: On the numerical solutions of Helmholtz's equation by the finite element method. SIAM J. Numer. Anal. **19**(5), 166–178 (1995)
7. Babuška, I.: The finite element method for elliptic equations with discontinuous coefficients. Computing (Arch. Elektron. Rechnen) **5**, 207–213 (1970)
8. Babuška, I.M., Sauter, S.A.: Is the pollution effect of the FEM avoidable for the Helmholtz equation considering high wave numbers? Comput. Math. Appl. **34**(6), 2392–2423 (1997)
9. Barrett, J.W., Elliott, C.M.: Fitted and unfitted finite-element methods for elliptic equations with smooth interfaces. IMA J. Numer. Anal. **7**(3), 283–300 (1987)
10. Bonnet-Ben Dhia, A.S., Ciarlet Jr., P., Zwölf, C.M.: Time harmonic wave diffraction problems in materials with sign-shifting coefficients. J. Comput. Appl. Math. **234**, 1912–1919 (2010)
11. Braess, D.: Finite Elements: Theory, Fast Solvers, and Applications in Solid Mechanics, 2nd edn. Cambridge University Press, Cambridge (2001). Translated from the 1992 German edition by Larry L. Schumaker
12. Bramble, J.H., King, J.T.: A finite element method for interface problems in domains with smooth boundaries and interfaces. Adv. Comput. Math. **6**(2), 109–138 (1996)
13. Brown, D.L.: A note on the numerical solution of the wave equation with piecewise smooth coefficients. Math. Comput. **42**(166), 369–391 (1984)
14. Burman, E., Wu, H., Zhu, L.: Linear continuous interior penalty finite element method for Helmholtz equation with high wave number: one-dimensional analysis. Numer. Methods Partial Differ. Equ. **32**(5), 1378–1410 (2016)
15. Bériot, H., Prinn, A., Gabard, G.: Efficient implementation of high-order finite elements for Helmholtz problems. Int. J. Numer. Methods Eng. **106**, 213–240 (2016)

16. Chandler-wilde, S.N., Zhang, B.: Scattering of electromagnetic waves by rough interfaces and inhomogeneous layers. SIAM J. Math. Anal. **30**(3), 559–583 (1989)
17. Chen, Z., Zou, J.: Finite element methods and their convergence for elliptic and parabolic interface problems. Numer. Math. **79**(2), 175–202 (1998)
18. Christiansen, P.S., Krenk, S.: A recursive finite element technique for acoustic fields in pipes with absorption. J. Sound Vib. **122**(1), 107–118 (1988)
19. Chu, C.-C., Graham, I.G., Hou, T.-Y.: A new multiscale finite element method for high-contrast elliptic interface problems. Math. Comput. **79**(272), 1915–1955 (2010)
20. Clough, R.W., Tocher, J.L.: Finite element stiffness matrices for analysis of plate bending. In: Przemieniecki, J.S., Bader,R.M., Bozich, W.F., Johnson, J.R., Mykytow, W.J. (eds.) Matrix Methods in Structural Mechanics, The Proceedings of the Conference held at Wright-Parrterson Air Force Base, Ohio, 26–28, October, 1965, pp. 515–545, Washington, 1966. Air Force Flight Dynamics Laboratory
21. Douglas Jr., J., Sheen, D., Santos, J.E.: Approximation of scalar waves in the space-frequency domain. Math. Models Methods Appl. Sci. **4**(4), 509–531 (1994)
22. Du, Y., Wu, H.: Preasymptotic error analysis of higher order FEM and CIP-FEM for Helmholtz equation with high wave number. SIAM J. Numer. Anal. **53**(2), 782–804 (2015)
23. Farhat, C., Harari, I., Hetmaniuk, U.: A discontinuous Galerkin method with lagrange multipliers for the solution of Helmholtz problems in the mid-frequency regime. Comput. Methods Appl. Mech. Eng. **192**, 1389–1419 (2003)
24. Feng, X., Wu, H.: Discontinuous Galerkin methods for the Helmholtz equation with large wave number. SIAM J. Numer. Anal. **47**(4), 2872–2896 (2009)
25. Gittelson, G., Hiptmair, R., Perugia, I.: Plane wave discontinuous Galerkin methods: analysis of the *h*-version. Esaim Math. Model. Numer. Anal. **43**, 297–331 (2009)
26. He, X., Lin, T., Lin, Y.: Approximation capability of a bilinear immersed finite element space. Numer. Methods Partial Differ. Equ. **24**(5), 1265–1300 (2008)
27. He, X., Lin, T., Lin, Y.: Interior penalty bilinear IFE discontinuous Galerkin methods for elliptic equations with discontinuous coefficient. J. Syst. Sci. Complex. **23**(3), 467–483 (2010)
28. He, X., Lin, T., Lin, Y.: Immersed finite element methods for elliptic interface problems with nonhomogeneous jump conditions. Int. J. Numer. Anal. Model. **8**(2), 284–301 (2011)
29. He, X., Lin, T., Lin, Y.: The convergence of the bilinear and linear immersed finite element solutions to interface problems. Numer. Methods Partial Differ. Equ. **28**(1), 312–330 (2012)
30. He, X., Lin, T., Lin, Y.: A selective immersed discontinuous Galerkin method for elliptic interface problems. Math. Methods Appl. Sci. **37**(7), 983–1002 (2014)
31. He, X.: Bilinear immersed finite elements for interface problems. PhD thesis, Virginia Polytechnic Institute and State University (2009)
32. Hou, T.Y., Wu, X.: A multiscale finite element method for elliptic problems in composite materials and porous media. J. Comput. Phys. **134**(1), 169–189 (1997)
33. Ihlenburg, F., Babuška, I.: Finite element solution of the Helmholtz equation with high wave number. I. The *h*-version of the FEM. Comput. Math. Appl. **30**(9), 9–37 (1995)
34. Ihlenburg, F., Babuška, I.: Finite element solutions of the Helmholtz equation with high wave number part II: the *h-p* version of the FEM. SIAM J. Numer. Anal. **34**(1), 315–358 (1997)
35. Jensen, F.B., Kuperman, W.A., Porter, M.B., Schmidt, H.: Computational Ocean Acoustics. Springer, Berlin (1995)
36. Klenow, B., Nisewonger, A., Batra, R.C., Brown, A.: Reflection and transmission of plane waves at an interface between two fluids. Comput. Fluids **36**, 1298–1306 (2007)
37. Kreiss, H., Petersson, N.A.: An embedded boundary method for the wave equation with discontinuous coefficients. SIAM J. Sci. Comput. **28**(6), 2054–2074 (2006)
38. Lam, C.Y., Shu, C.-W.: A phase-based interior penalty discontinuous Galerkin method for the Helmholtz equation with spatially varying wavenumber. Comput. Methods Appl. Mech. Eng. **318**, 456–473 (2017)
39. LeVeque, R.J., Li, Z.L.: The immersed interface method for elliptic equations with discontinuous coefficients and singular sources. SIAM J. Numer. Anal. **31**(4), 1019–1044 (1994)
40. Li, Z., Ito, K.: The Immersed Interface Method: Numerical Solutions of PDEs Involving Interfaces and Irregular Domains. Frontiers in Applied Mathematics, vol. 33. Society for Industrial and Applied Mathematics (SIAM), Philadelphia (2006)
41. Li, Z., Lin, T., Lin, Y., Rogers, R.C.: An immersed finite element space and its approximation capability. Numer. Methods Partial Differ. Equ. **20**(3), 338–367 (2004)
42. Li, Z., Lin, T., Wu, X.: New Cartesian grid methods for interface problems using the finite element formulation. Numer. Math. **96**(1), 61–98 (2003)

43. Lin, T., Lin, Y., Rogers, R., Lynne Ryan, M.: A Rectangular Immersed Finite Element Space for Interface Problems. Scientific Computing and Applications (Kananaskis, AB, 2000). Advances in Computation: Theory and Practice, vol. 7, pp. 107–114. Nova Sci. Publ, Huntington (2001)
44. Lin, T., Lin, Y., Zhang, X.: Partially penalized immersed finite element methods for elliptic interface problems. SIAM J. Numer. Anal. **53**(2), 1121–1144 (2015)
45. Lin, T., Yang, Q., Zhang, X.: A priori error estimates for some discontinuous Galerkin immersed finite element methods. J. Sci. Comput. **65**, 875–894 (2015)
46. Parsania, A., Melenk, J.M., Sauter, D.: General DG-methods for highly indefinite Helmholtz problems. J. Sci. Comput. **57**, 536–581 (2013)
47. Perugia, I.: A note on the discontinuous Galerkin approximation of the Helmholtz equation. Lecture notes. ETH, Zürich (2006)
48. Romdhane, M.B.: Higher-degree immersed finite elements for second-order elliptic interface problems. PhD thesis, Virginia Polytechnic Institute and State University (2011)
49. Semblat, J.F., Brioist, J.J.: Efficiency of higher order finite elements for the analysis of seismic wave propagation. J. Sound Vib. **231**(2), 460–467 (2000)
50. Speck, F.O.: Sommerfeld diffraction problems with first and second kind boundary conditions. SIAM J. Math. Anal. **20**(2), 396–407 (1989)
51. Suater, S.A., Warnke, R.: Composite finite elements for elliptic boudnary value problems with discontinuous coefficients. Computing **77**, 29–55 (2006)
52. Wang, K., Wong, Y.: Pollution-free finite difference schemes for non-homogeneous Helmholtz equation. Int. J. Numer. Anal. Model. **11**(4), 787–815 (2014)
53. Xu, J.: Estimate of the convergence rate of the finite element solutions to elliptic equation of second order with discontinuous coefficients. Nat. Sci. J. Xiangtan Univ. **1**, 1–5 (1982)
54. Zhang, J.: Wave propagation across fluid-solid interfaces: a grid method approach. Geophys. J. Int. **159**, 240–252 (2004)
55. Zhang, S.M., Li, Z.: An augmented IIM for Helmholtz/Poisson equations on irregular domains in complex space. Int. J. Numer. Anal. Model. **13**(1), 166–178 (2016)
56. Zhang, X.: Nonconforming immersed finite element methods for interface problems. PhD thesis, Virginia Polytechnic Institute and State University (2013)
57. Zou, Z., Aquino, W., Harari, I.: Nitsche's method for Helmholtz problems with embedded interfaces. Int. J. Numer. Meth. Eng. **110**, 618–636 (2017)